Finite-temperature screening and the specific heat of doped graphene sheets

2009 J. Phys. A: Math. Theor. 42 214015

(http://iopscience.iop.org/1751-8121/42/21/214015)

IOP PUBLISHING JOURNAL OF PHYSICS A: MATHEMATICAL AND THEORETICAL

J. Phys. A: Math. Theor. **42** (2009) 214015 (9pp) doi:10.1088/1751-8113/42/21/214015

Finite-temperature screening and the specific heat of doped graphene sheets

M R Ramezanali[1], M M Vazifeh[1], Reza Asgari[2], Marco Polini[3] and A H MacDonald[4]

[1] Department of Physics, Sharif University of Technology, Tehran 11155-9161, Iran
[2] School of Physics, Institute for research in fundamental sciences, IPM 19395-5531 Tehran, Iran
[3] NEST-CNR-INFM and Scuola Normale Superiore, I-56126 Pisa, Italy
[4] Department of Physics, The University of Texas at Austin, Austin, TX 78712, USA

E-mail: asgari@theory.ipm.ac.ir and m.polini@sns.it

Received 11 November 2008, in final form 16 February 2009
Published 8 May 2009
Online at stacks.iop.org/JPhysA/42/214015

Abstract

At low energies, electrons in doped graphene sheets are described by a massless Dirac fermion Hamiltonian. In this work, we present a semi-analytical expression for the dynamical density–density linear-response function of non-interacting massless Dirac fermions (the so-called 'Lindhard' function) at finite temperature. This result is crucial to describe finite-temperature screening of interacting massless Dirac fermions within the random phase approximation. In particular, we use it to make quantitative predictions for the specific heat and the compressibility of doped graphene sheets. We find that, at low temperatures, the specific heat has the usual normal-Fermi-liquid linear-in-temperature behavior, with a slope that is solely controlled by the renormalized quasiparticle velocity.

PACS numbers: 71.10.−w, 71.45.Gm, 72.10.−d

(Some figures in this article are in colour only in the electronic version)

1. Introduction

Graphene is a newly realized two-dimensional (2D) electron system that has attracted a great deal of interest in the scientific community because of the new physics which it exhibits and because of its potential as a new material for electronic technology [1, 2]. The agent responsible for many of the interesting electronic properties of graphene sheets is the non-Bravais honeycomb-lattice arrangement of carbon atoms, which leads to a gapless semiconductor with valence and conduction π-bands. States near the Fermi energy of a graphene sheet are described by a spin-independent massless Dirac Hamiltonian [3],

$$\mathcal{H}_{\rm D} = v_{\rm F}\, \boldsymbol{\sigma}\cdot\boldsymbol{p}, \tag{1}$$

where v_F is the Fermi velocity, which is density independent and roughly 300 times smaller than the velocity of light in the vacuum and $\boldsymbol{\sigma} = (\sigma^x, \sigma^y)$ is a vector constructed with two Pauli matrices $\{\sigma^i, i = x, y\}$, which operate on pseudospin (sublattice) degrees of freedom. Note that the eigenstates of $\mathcal{H}_D$ have a definite *chirality* rather than a definite pseudospin, i.e., they have a definite projection of the honeycomb-sublattice pseudospin onto the momentum $\boldsymbol{p}$.

When non-relativistic Coulombic electron–electron interactions are added to the kinetic Hamiltonian (1), graphene represents a new type of many-electron problem, distinct from both an ordinary 2D electron gas (EG) and quantum electrodynamics. The Dirac-like wave equation and the chirality of its eigenstates lead indeed to both unusual electron–electron interaction effects [4–8] and unusual response to external potentials [9–11]. For example, Friedel oscillations in the charge density around an impurity show a faster decay [$\delta n(\boldsymbol{r}) \sim r^{-3}$] than in a conventional 2D EG [9].

Within this low-energy description, the properties of doped graphene sheets depend on the dimensionless coupling constant

$$\alpha_{gr} = g\frac{e^2}{\epsilon\hbar v_F} \tag{2}$$

and on an ultraviolet cut-off $\Lambda = k_c/k_F$. Here $g = g_s g_v = 4$ accounts for spin and valley degeneracy, $k_F = (4\pi n/g)^{1/2}$ is the Fermi wave number with n being the electron density and k_c should be assigned a value corresponding to the wavevector range over which the continuum model (1) describes graphene. For definiteness, we take k_c to be such that $\pi k_c^2 = (2\pi)^2/\mathcal{A}_0$, where $\mathcal{A}_0 = 3\sqrt{3}a_0^2/2$ is the area of the unit cell in the honeycomb lattice, with $a_0 \simeq 1.42$ Å the carbon–carbon distance. With this choice

$$\Lambda = \frac{\sqrt{g}}{\sqrt{n\mathcal{A}_0}}. \tag{3}$$

The continuum model is useful when $k_c \gg k_F$, i.e. when $\Lambda \gg 1$.

Vafek [12] has recently shown that the specific heat of undoped graphene sheets presents an anomalous low-temperature behavior showing a logarithmic suppression with respect to its non-interacting counterpart, $\lim_{T\to 0} C_V/C_V^{(0)} \propto 1/\ln(T)$. On the other hand, in [6, 7] we have demonstrated (see also [8]) that doped graphene sheets are normal (pseudochiral) Fermi liquids, with Landau parameters that possess, however, a quite distinct behavior from those of conventional 2D EGs. In this work, we calculate the Helmholtz free energy $\mathcal{F}(T)$ of doped graphene sheets within the random phase approximation (RPA) [13, 14]. This allows us to access important thermodynamic quantities, such as the compressibility and the specific heat, which can be calculated by taking appropriate derivatives of the free energy. We show that, at low temperatures, the specific heat of doped graphene, contrary to that of the undoped system [12], has the usual linear-in-temperature behavior, which is solely controlled by the renormalized velocity of quasiparticles as in a normal Fermi liquid.

2. The Helmoltz free energy and the Lindhard response function at finite temperature

The free energy $\mathcal{F} = \mathcal{F}_0 + \mathcal{F}_{int}$ is usually decomposed into the sum of a non-interacting term $\mathcal{F}_0$ and an interaction contribution $\mathcal{F}_{int}$. To evaluate the interaction contribution to the Helmholtz free energy we follow a familiar strategy [14] by combining a coupling constant integration expression for $\mathcal{F}_{int}$ valid for uniform continuum models ($\hbar = 1$ from now on),

$$\mathcal{F}_{int}(T) = \frac{N}{2}\int_0^1 d\lambda \int \frac{d^2\boldsymbol{q}}{(2\pi)^2} v_q [S^{(\lambda)}(q, T) - 1] \tag{4}$$

with a fluctuation–dissipation-theorem (FDT) expression [14] for the static structure factor:

$$S^{(\lambda)}(q,T) = -\frac{1}{\pi n}\int_0^{+\infty} \mathrm{d}\omega \coth(\beta\omega/2)\mathrm{Im}\,\chi^{(\lambda)}_{\rho\rho}(q,\omega,T). \tag{5}$$

Here $v_q = 2\pi e^2/(\epsilon q)$ is the 2D Fourier transform of the Coulomb potential and $\beta = (k_\mathrm{B}T)^{-1}$. We anticipate that this version of the FDT (in which the frequency integration has to be performed over the real-frequency axis) requires care in handling the plasmon contribution to $\mathcal{F}_{\mathrm{int}}(T)$ (see the discussion below).

The RPA approximation for $\mathcal{F}_{\mathrm{int}}$ then follows from the RPA approximation for $\chi^{(\lambda)}_{\rho\rho}(q,\omega)$,

$$\chi^{(\lambda)}_{\rho\rho}(q,\omega,T) = \frac{\chi^{(0)}(q,\omega,T)}{1-\lambda v_q \chi^{(0)}(q,\omega,T)}, \tag{6}$$

where $\chi^{(0)}(q,\omega,T)$ is the non-interacting density–density response function:

$$\chi^{(0)}(q,\omega,T) = g\lim_{\eta\to 0^+}\sum_{s,s'=\pm}\int \frac{\mathrm{d}^2\boldsymbol{k}}{(2\pi)^2}\frac{1+ss'\cos(\theta_{\boldsymbol{k},\boldsymbol{k}+\boldsymbol{q}})}{2}\frac{n_\mathrm{F}(\varepsilon_{\boldsymbol{k},s})-n_\mathrm{F}(\varepsilon_{\boldsymbol{k}+\boldsymbol{q},s'})}{\omega+\varepsilon_{\boldsymbol{k},s}-\varepsilon_{\boldsymbol{k}+\boldsymbol{q},s'}+\mathrm{i}\eta}. \tag{7}$$

Here $\varepsilon_{\boldsymbol{k},s} = sv_\mathrm{F}k$ are the Dirac band energies and $n_\mathrm{F}(\varepsilon) = \{\exp[\beta(\varepsilon-\mu_0)]+1\}^{-1}$ is the usual Fermi–Dirac distribution function, $\mu_0 = \mu_0(T)$ being the non-interacting chemical potential. As usual, this is determined by the normalization condition

$$n = \int_{-\infty}^{+\infty}\mathrm{d}\varepsilon\nu(\varepsilon)n_\mathrm{F}(\varepsilon), \tag{8}$$

where $\nu(\varepsilon) = g\varepsilon/\left(2\pi v_\mathrm{F}^2\right)$ is the non-interacting density of states. For $T\to 0$ one finds $\mu_0(T) = \varepsilon_\mathrm{F} - \pi^2(T/T_\mathrm{F})^2/6$, where $T_\mathrm{F} = \varepsilon_\mathrm{F}/k_B$ is the Fermi temperature. The factor in the first line of equation (7), which depends on the angle $\theta_{\boldsymbol{k},\boldsymbol{k}+\boldsymbol{q}}$ between $\boldsymbol{k}$ and $\boldsymbol{k}+\boldsymbol{q}$, describes the dependence of Coulomb scattering on the relative chirality ss' of the interacting electrons.

After some straightforward algebraic manipulations, we arrive at the following expressions for the imaginary $[\mathrm{Im}\,\chi^{(0)}(q,\omega,T)]$ and real $[\mathrm{Re}\,\chi^{(0)}(q,\omega,T)]$ parts of the non-interacting density–density response function for $\omega > 0$:

$$\begin{aligned}\mathrm{Im}\,\chi^{(0)}(q,\omega,T) = \frac{g}{4\pi}\sum_{\alpha=\pm}\Big\{&\Theta(v_\mathrm{F}q-\omega)q^2 f(v_\mathrm{F}q,\omega)\big[G^{(\alpha)}_+(q,\omega,T)-G^{(\alpha)}_-(q,\omega,T)\big]\\ &+\Theta(\omega-v_\mathrm{F}q)q^2 f(\omega,v_\mathrm{F}q)\left[-\frac{\pi}{2}\delta_{\alpha,-}+H^{(\alpha)}_+(q,\omega,T)\right]\Big\}\end{aligned} \tag{9}$$

and

$$\begin{aligned}\mathrm{Re}\,\chi^{(0)}(q,\omega,T) = \frac{g}{4\pi}\sum_{\alpha=\pm}\Bigg\{&\frac{-2k_\mathrm{B}T\ln[1+e^{\alpha\mu_0/(k_\mathrm{B}T)}]}{v_\mathrm{F}^2}+\Theta(\omega-v_\mathrm{F}q)\\ &\times q^2 f(\omega,v_\mathrm{F}q)\big[G^{(\alpha)}_-(q,\omega,T)-G^{(\alpha)}_+(q,\omega,T)\big]\\ &+\Theta(v_\mathrm{F}q-\omega)q^2 f(v_\mathrm{F}q,\omega)\left[-\frac{\pi}{2}\delta_{\alpha,-}+H^{(\alpha)}_-(q,\omega,T)\right]\Bigg\}.\end{aligned} \tag{10}$$

Here

$$f(x,y) = \frac{1}{2\sqrt{x^2-y^2}}, \tag{11}$$

$$G^{(\alpha)}_\pm(q,\omega,T) = \int_1^\infty \mathrm{d}u\,\frac{\sqrt{u^2-1}}{\exp\left(\frac{|v_\mathrm{F}qu\pm\omega|-2\alpha\mu_0}{2k_\mathrm{B}T}\right)+1} \tag{12}$$

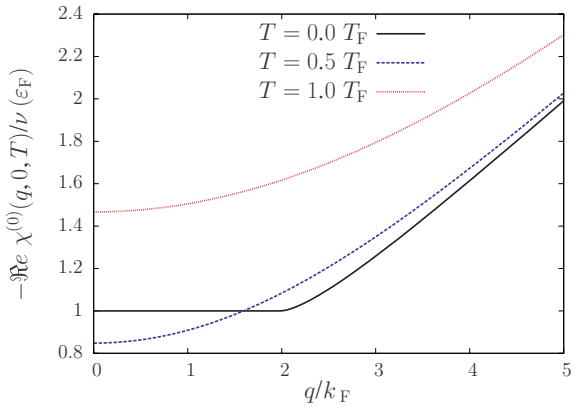

Figure 1. The static response function Re $\chi^{(0)}(q, 0, T)$ (in units of $-\nu(\varepsilon_F)$) as a function of q/k_F for three values of $0 \leqslant T/T_F \leqslant 1$. Note the non-monotonic behavior of this quantity for $q \lesssim k_F$.

and

$$H_{\pm}^{(\alpha)}(q, \omega, T) = \int_{-1}^{1} du \frac{\sqrt{1-u^2}}{\exp\left(\frac{|v_F q u \pm \omega| - 2\alpha\mu_0}{2k_B T}\right) + 1}. \tag{13}$$

These semi-analytical expressions for Re $\chi^{(0)}(q, \omega, T)$ and Im $\chi^{(0)}(q, \omega, T)$ constitute the first important result of this work. In the limit $T \to 0$, it is possible to show that equations (9) and (10) reduce to the well-known zero-temperature results [15]. In figure 1, we have plotted the static response, Re $\chi^{(0)}(q, 0, T)$, as a function of q/k_F for different values of T/T_F. The non-monotonic behavior of Re $\chi^{(0)}(q, 0, T)$ originates from a competition between intra- and inter-band contributions to this quantity. For every fixed q indeed, the intra-band contribution *decreases* rapidly with increasing T, while the inter-band contribution *increases* quickly at small T and then more slowly (in an essentially linear fashion) at large T. The competition between the intra- and inter-band contributions to $\partial[\text{Re}\,\chi^{(0)}(q, 0, T)]/\partial T$ for $T \ll T_q^{\text{cross}}$ [5] is responsible for the non-monotonic behavior of Re $\chi^{(0)}(q, 0, T)$ illustrated in figure 1.[6] A study of the temperature-dependence of the static non-interacting density–density response function that reaches identical conclusions has appeared recently in the literature [16]. The temperature dependence of the Lindhard function at a finite frequency is instead presented in figure 2. An illustrative plot of the imaginary part of the inverse RPA dielectric function $\varepsilon(q, \omega, T) = 1 - v_q \chi^{(0)}(q, \omega, T)$ is shown in figure 3.

The coupling constant integration in equation (4) can be carried out partly analytically due to the simple RPA expression (6). We find that the interaction contribution to the free energy per particle $f_{\text{int}}(T)$ is given by

$$f_{\text{int}}(T) \equiv \frac{\mathcal{F}_{\text{int}}(T)}{N} = \frac{1}{2}\int \frac{d^2\boldsymbol{q}}{(2\pi)^2}\left\{-\frac{1}{\pi n}\int_0^{+\infty} d\omega \coth(\beta\omega/2) \times \arctan\left[\frac{v_q\,\text{Im}\,\chi^{(0)}(q, \omega, T)}{1 - v_q\,\text{Re}\,\chi^{(0)}(q, \omega, T)}\right] - v_q\right\}$$

[5] Here T_q^{cross} is a q-dependent temperature scale at which intra- and inter-band contributions to Re $\chi^{(0)}(q, 0, T)$ are equal.

[6] For $T \gg T_q^{\text{cross}}$ the inter-band contribution is much larger than the intra-band one. However, $\partial[\text{Re}\,\chi^{(0)}_{\text{intra}}(q, 0, T)]/\partial T$ is negative and large in absolute value and dominates over $\partial[\text{Re}\,\chi^{(0)}_{\text{inter}}(q, 0, T)]/\partial T$, establishing eventually the usual monotonic behavior characteristic of the conventional 2D EG.

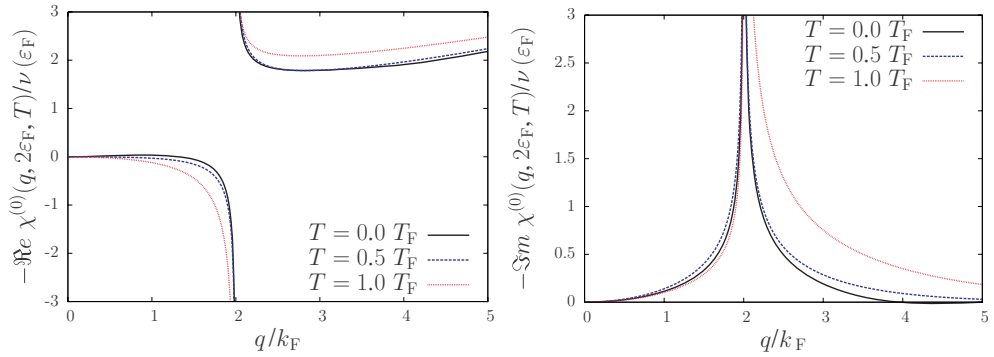

Figure 2. Left panel: the real part of the dynamical response function Re $\chi^{(0)}(q, \omega, T)$ (in units of $-\nu(\varepsilon_F)$) as a function of q/k_F for $\omega = 2\varepsilon_F$ and three values of $0 \leqslant T/T_F \leqslant 1$. Right panel: same as in the left panel but for the imaginary part.

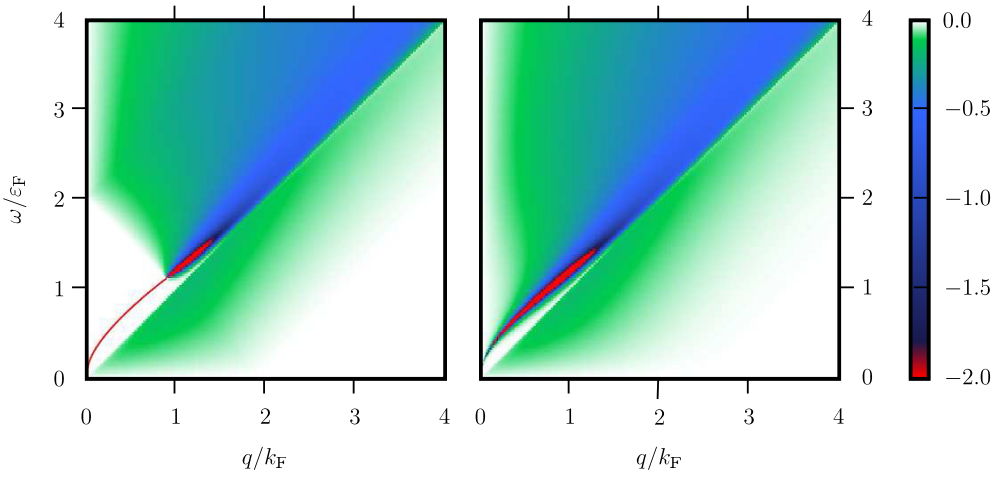

Figure 3. Left panel: Im $[\varepsilon^{-1}(q, \omega, T)]$ as a function of q/k_F and ω/ε_F for $\alpha_{gr} = 2$ and $T = 0$. The red solid line is the plasmon dispersion relation. Right panel: same as in the left panel but for $T = 0.2T_F$ (corresponding roughly to room temperature).

$$+\frac{1}{2n}\int\frac{\mathrm{d}^2\boldsymbol{q}}{(2\pi)^2}\int_0^1\frac{\mathrm{d}\lambda}{\lambda}\coth(\beta\omega_{\mathrm{pl}}/2)\mathrm{Re}\,\chi^{(0)}(q,\omega_{\mathrm{pl}},T)$$
$$\times\left|\frac{\partial[\mathrm{Re}\,\chi^{(0)}(q,\omega,T)]}{\partial\omega}\right|^{-1}_{\omega=\omega_{\mathrm{pl}}}. \tag{14}$$

In this equation, the first term comes from the smooth electron–hole contribution to Im $\chi^{(\lambda)}_{\rho\rho}$, while the second term comes from the plasmon contribution; $\omega_{\mathrm{pl}} = \omega_{\mathrm{pl}}(q, T, \lambda)$ is the plasmon dispersion relation at the coupling constant λ which can be found numerically by solving the equation $1 - \lambda v_q$ Re $\chi^{(0)}(q, \omega, T) = 0$. Note that in a usual 2D EG, the exchange energy starts to matter little for T of order T_F because all the occupation numbers are small and the Pauli exclusion principle matters little. In the graphene case, however, exchange interactions with the negative energy sea remain important as long as T is small compared to $v_F k_c/k_B = T_F\Lambda$.

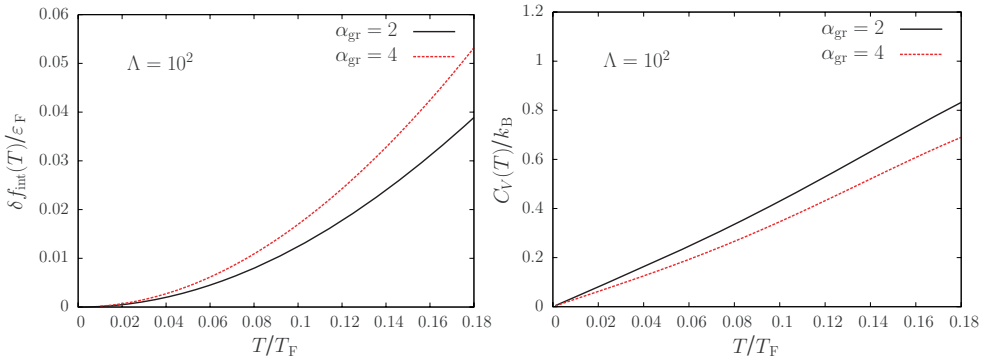

Figure 4. Left panel: the (regularized) interaction contribution to the free energy $\delta f_{\rm int}(T)$ (in units of the Fermi energy $\varepsilon_{\rm F}$) as a function of $T/T_{\rm F}$ for $\Lambda = 10^2$. Right panel: the specific heat $C_V(T)$ (in units of $k_{\rm B}$) as a function of $T/T_{\rm F}$.

The free energy calculated according to equation (14) is divergent since it includes the interaction energy of the model's infinite sea of negative energy particles. Following Vafek [12], we choose the free energy at $T = 0$, $f(T = 0)$, as our 'reference' free energy, and thus introduce the regularized quantity $\delta f \equiv f(T) - f(T = 0)$. This again can be decomposed into the sum of a non-interacting contribution, $\delta f_0(T \to 0) = -g\varepsilon_{\rm F}\pi^2(T/T_{\rm F})^2/12$, and an interaction-induced contribution $\delta f_{\rm int}(T) = f_{\rm int}(T) - f_{\rm int}(T = 0)$, which can be calculated from equation (14). Numerical results for $\delta f_{\rm int}(T)$ as a function of the reduced temperature $T/T_{\rm F}$ are shown in the left panel of figure 4.

The low-temperature behavior of the interaction contribution to the free energy can be extracted analytically with some patience. After some lengthy but straightforward algebra we find, to leading order in Λ,

$$\delta f_{\rm int}(T \to 0) = \varepsilon_{\rm F}\frac{\pi^2}{3}\left(\frac{T}{T_{\rm F}}\right)^2 \frac{\alpha_{\rm gr}[1 - \alpha_{\rm gr}\xi(\alpha_{\rm gr})]}{4g} \ln\Lambda + \text{R.T.}, \tag{15}$$

where the function $\xi(x)$, defined as in equation (14) of [6], is given by $\xi(x) = 128/(\pi^2 x^3) - 32/(\pi^2 x^2) + 1/x - h(\pi x/8)$ with

$$h(x) = \begin{cases} \dfrac{1}{2x^3\sqrt{1-x^2}} \arctan\left(\dfrac{\sqrt{1-x^2}}{x}\right) & \text{for} \quad x < 1 \\ \dfrac{1}{4x^3\sqrt{x^2-1}} \ln\left(\dfrac{x+\sqrt{x^2-1}}{x-\sqrt{x^2-1}}\right) & \text{for} \quad x > 1. \end{cases} \tag{16}$$

The symbol 'R.T.' in the lfs of equation (15) indicates 'regular terms', i.e. terms that, by definition, are finite in the limit $\Lambda \to \infty$. Equation (15) represents the second important result of this work.

Before concluding this section, we remind the reader that in [6] it has been proven that the renormalized RPA quasiparticle velocity $v^\star$ is given, at weak coupling and to leading order in Λ, by

$$\frac{v^\star}{v_{\rm F}} = 1 + \frac{\alpha_{\rm gr}[1 - \alpha_{\rm gr}\xi(\alpha_{\rm gr})]}{4g} \ln\Lambda. \tag{17}$$

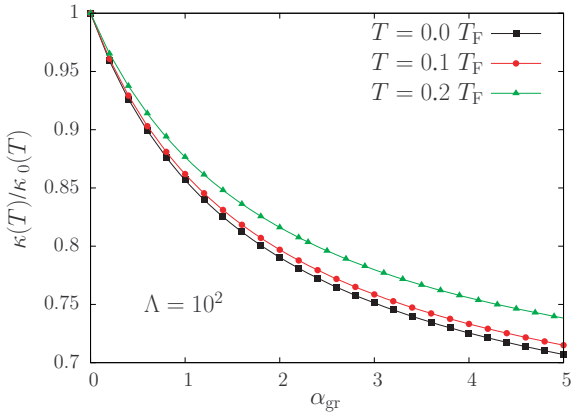

Figure 5. The dimensionless ratio $\kappa(T)/\kappa_0(T)$ as a function of graphene's coupling constant α_{gr} for three values of $0 \leqslant T/T_F \leqslant 0.2$.

3. The specific heat and the compressibility

The specific heat can be calculated from the second derivative of the Helmholtz free energy, $C_V = -T\partial^2[n\delta f(T)]/\partial T^2$.[7] Numerical results for $C_V(T)$ as a function of temperature are shown in figure 4. We thus see that $\delta f_{int}(T \to 0) \propto T^2$ in equation (15) implies a conventional Fermi-liquid behavior with a linear-in-T specific heat. Moreover, comparing equation (15) with equation (17) we find that the ratio between C_V and its non-interacting value $C_V^{(0)}$ is given by

$$\lim_{T\to 0} \frac{C_V}{C_V^{(0)}} = \frac{v_F}{v^\star}, \tag{18}$$

a well-known property of normal Fermi liquids [13, 14]. We are thus led to conclude, in full agreement with the zero-temperature calculations of the quasiparticle energy and lifetime performed in [6, 7], that doped graphene sheets are normal Fermi liquids. Note that the fact that interactions enhance the quasiparticle velocity (see equation (17)) implies that the specific heat of doped graphene sheets is *suppressed* with respect to its non-interacting value.

The compressibility can be calculated from the following equation:

$$\frac{1}{n^2\kappa(T)} = \frac{1}{n^2\kappa_0(T)} + \frac{\partial^2[n\delta f_{int}(T)]}{\partial n^2}, \tag{19}$$

where $\kappa_0^{-1}(T)$ is the inverse compressibility of the non-interacting system at finite temperature. In the low-temperature limit $1/[n^2\kappa_0(T \to 0)] = n\varepsilon_F/2 + gn\varepsilon_F\pi^2(T/T_F)^2/48$. The dependence of the ratio $\kappa(T)/\kappa_0(T)$ on α_{gr} and T/T_F is shown in figure 5.

4. Conclusions

In this work, we have presented semi-analytical expressions for the real and imaginary parts of the density–density linear-response function of non-interacting massless Dirac fermions at finite temperature. These results are very useful to study finite-temperature screening within

[7] The second derivative is calculated using the full temperature dependent free-energy of the non-interacting system, $\delta f_0(T)$, and not its analytical expression reported above that is valid only for $T \ll T_F$.

the random phase approximation. For example, they can be used to calculate the conductivity at finite temperature within Boltzmann transport theory and make quantitative comparison with recent experimental results in unsuspended [17, 18] and suspended graphene sheets [19, 20] (see also comments in [9, 16]).

The Lindhard function at finite temperature is also extremely useful to calculate finite-temperature equilibrium properties of interacting massless Dirac fermions, such as the specific heat and the compressibility. For example, in this work we have been able to show that, at low temperatures, the specific heat of interacting massless Dirac fermions has the usual normal-Fermi-liquid linear-in-temperature behavior, with a slope that is solely controlled by the renormalized quasiparticle velocity.

Acknowledgments

MP was partly supported by the CNR-INFM 'Seed Projects'. AHM was supported by the Welch Foundation and SWAN-NRI.

References

[1] Geim A K and Novoselov K S 2007 The rise of graphene *Nature Mater.* **6** 183
2007 Exploring graphene—recent research advances *Solid State Communication* vol 143 ed S Das Sarma, A K Geim, P Kim and A H MacDonald
Castro Neto A H, Guinea F, Peres N M R, Novoselov K S and Geim A K 2009 The electronic properties of graphene *Rev. Mod. Phys.* **81** 109

[2] For a recent popular review see, Geim A K and MacDonald A H 2007 Graphene: exploring carbon flatland *Phys. Today* **60** 35

[3] Slonczewski J C and Weiss P R 1958 Band structure of graphite *Phys. Rev.* **109** 272
Ando T, Nakanishi T and Saito R 1998 Berry's phase and absence of back scattering in carbon nanotubes *J. Phys. Soc. Japan* **67** 2857

[4] González J, Guinea F and Vozmediano M A 1996 Unconventional quasiparticle lifetime in graphite *Phys. Rev. Lett.* **77** 3589
Gonzáles J, Guinea F and Vozmediano M A 1999 Marginal-Fermi-liquid behavior from two-dimensional Coulomb interaction *Phys. Rev.* B **59** R2474

[5] Barlas Y, Pereg-Barnea T, Polini M, Asgari R and MacDonald A H 2007 Chirality and correlations in graphene *Phys. Rev. Lett.* **98** 236601

[6] Polini M, Asgari R, Barlas Y, Pereg-Barnea T and MacDonald A H 2007 Graphene: a pseudochiral Fermi liquid *Solid. State Commun.* **143** 58

[7] Polini M, Asgari R, Borghi G, Barlas Y, Pereg-Barnea T and MacDonald A H 2008 Plasmons and the spectral function of graphene *Phys. Rev.* B **77** 081411

[8] Hwang E H and Das Sarma S 2007 Dielectric function, screening, and plasmons in two-dimensional graphene *Phys. Rev.* B **75** 205418
Das Sarma S, Hwang E H and Tse W-K 2007 Many-body interaction effects in doped and undoped graphene: Fermi liquid versus non-Fermi liquid *Phys. Rev.* B **75** 121406
Hwang E H, Hu B Y-K and Das Sarma S 2007 Inelastic carrier lifetime in graphene *Phys. Rev.* B **76** 115434
Hwang E H, Hu B Y-K and Das Sarma S 2007 Density dependent exchange contribution to $\partial\mu/\partial n$ and compressibility in graphene *Phys. Rev. Lett.* **99** 226801

[9] Cheianov V V and Fal'ko V I 2006 Friedel oscillations, impurity scattering, and temperature dependence of resistivity in graphene *Phys. Rev. Lett.* **97** 226801

[10] Polini M, Tomadin A, Asgari R and MacDonald A H 2008 Density functional theory of graphene sheets *Phys. Rev.* B **78** 115426

[11] Rossi E and Das Sarma S 2008 Ground state of graphene in the presence of random charged impurities *Phys. Rev. Lett.* **101** 166803

[12] Vafek O 2007 Anomalous thermodynamics of Coulomb-interacting massless Dirac fermions in two spatial dimensions *Phys. Rev. Lett.* **98** 216401

[13] Pines D and Noziéres P 1966 *The Theory of Quantum Liquids* (Menlo Park: Addison-Wesley)

[14] Giuliani G F and Vignale G 2005 *Quantum Theory of the Electron Liquid* (Cambridge: Cambridge University Press)
[15] See for example, Wunsch B, Stauber T, Sols F and Guinea F 2006 Dynamical polarization of graphene at finite doping *New J. Phys.* **8** 318
[16] Hwang E H and Das Sarma S 2008 Screening induced temperature dependent transport in 2D graphene, arXiv:0811.1212v1
[17] Morozov S V, Novoselov K S, Katsnelson M I, Schedin F, Elias D C, Jaszczak J A and Geim A K 2008 Giant intrinsic carrier mobilities in graphene and its bilayer *Phys. Rev. Lett.* **100** 016602
[18] Chen J H, Jang C, Xiao S, Ishigami M and Fuhrer M S 2008 Intrinsic and extrinsic performance limits of graphene devices on SiO_2 *Nature Nanotech.* **3** 206
[19] Bolotin K I, Sikes K J, Hone J, Stormer H L and Kim P 2008 Temperature-dependent transport in suspended graphene *Phys. Rev. Lett.* **101** 096802
[20] Du X, Skachko I, Barker A and Andrei E Y 2008 Approaching ballistic transport in suspended graphene *Nature Nanotech.* **3** 491